JOURNAL OF GEOPHYSICAL RESEARCH, VOL. 105, NO. A12, PAGES 27,239–27,249, DECEMBER 1, 2000

Model for the mass fractionation in the January 6, 1997, coronal mass ejection

Peter Wurz and Peter Bochsler
Physics Institute, University of Bern, Bern, Switzerland

Martin A. Lee
Institute for the Study of Earth, Oceans and Space and Department of Physics, University of New Hampshire, Durham, USA

Abstract. For the coronal mass ejection (CME) of January 6, 1997, strong element fractionation of the heavy ions was observed at 1 AU with the Mass Time-of-Flight (MTOF) sensor of the Charge, Element, and Isotope Analysis System (CELIAS) on the Solar and Heliospheric Observatory (SOHO). During the passage of the CME plasma and the passage of the erupted filament, which followed the CME, a mass-dependent element fractionation was found with an enhancement of heavy elements, increasing monotonically with atomic mass. Si/O and Fe/O ratios around 0.5 were observed, which corresponds to an increase of about a factor of 4 compared to regular slow solar wind. We present a theoretical model with which we can reproduce the observed element fractionation. The model assumes hot coronal loops with non-Maxwellian electron distributions as the precursor structure of the CME on the solar surface. Diffusion perpendicular to the magnetic field results in the preferential loss of lighter ions from the loop, leading to mass fractionation. To quantitatively reproduce the fractionation process, the loops must have existed for $\sim$ 28 hours before they became part of the CME plasma, a time that is commensurate with optical observations of loops in the active region from which the CME was launched.

1. Introduction

In this paper we present a theoretical model to explain the elemental fractionation reported for the plasma of the coronal mass ejection (CME) of January 6, 1997, using data from the Mass Time-of-Flight (MTOF) sensor of the Charge, Element, and Isotope Analysis System (CELIAS) on the Solar and Heliospheric Observatory (SOHO) mission [*Wurz et al.*, 1997, 1998]. The CME originated on the solar surface around 1500 UT on January 6, 1997, and arrived at the SOHO spacecraft on January 10, 1997, at 0411 UT. Approximately 30 min later it passed the location of the Wind spacecraft (on January 10, 1997, at 0448 UT). An overview of this CME event has been given by [*Fox et al.*, 1998], which covers the launch of the CME, its propagation through interplanetary space, and its effect on the Earth's magnetosphere. A review covering the present understanding of CMEs has been given recently by [*Gosling*, 1997]. From the magnetic field measurements on Wind it has been concluded that this CME falls into the group of magnetic cloud events [*Burlaga et al.*, 1998]. Observational signatures of magnetic clouds consist of an enhanced magnetic field strength, a smooth rotation of the magnetic field direction as the cloud passes the spacecaft, and a low proton temperature. It has been found earlier that near 1 AU about one third of all CMEs in the ecliptic plane are magnetic cloud events [*Gosling*, 1990].

The CME was slightly faster than the preceding solar wind and created a shock that was observed at SOHO on January 10, 1997, at 0022 UT. The CME was followed by coronal-hole-type solar wind, which arrived at the position of the SOHO spacecraft on January 11 at 0656 UT. Just before the arrival of the coronal-hole-type solar wind a pronounced increase in the proton density was observed, which was attributed to an erupting filament (solar prominence material) on the solar surface [*Burlaga et al.*, 1998]. Wind/SWE results indicate that the proton density was about 185 cm^{-3} in the spike resulting from the filament eruption, a value which is about a factor of 20 above typical proton densities in the slow solar wind and probably is the highest solar wind proton density ever observed at Earth orbit.

The analysis of the heavy ions in the CME and filament plasmas revealed an unusual composition [*Wurz et al.*, 1998]. During the passage of the CME plasma and the passage of the erupted filament, which followed

Paper number 2000JA900120.
0148-0227/00/2000JA900120$09.00

the CME, a mass-dependent element fractionation was found with a strong enhancement of heavy elements, increasing monotonically with atomic mass. Si/O and Fe/O ratios around 0.5 were observed, which is highly unusual and corresponds to an increase of about a factor of 4 compared to regular slow solar wind. One possible explanation for the unusual elemental composition of the CME and the filament plasma is that an isolated volume of material, the precursor of the CME, and the erupting filament, resided on the solar surface where matter boiled off from the volume. Given the gravitational field of the Sun, lighter elements would be lost more easily than heavier ones and a mass-dependent change of composition would result if the volume was isolated for a sufficiently long time on the solar surface. It has been observed frequently that a CME begins as a slow swelling of a coronal streamer on timescales of several days [*Hundhausen*, 1999]. Once this isolated volume is released from the solar surface in the form of a CME or an erupting filament, it will carry its altered composition into interplanetary space. Another explanation for the unusual composition could involve fractionation by selective acceleration after the release of the isolated volume. The mass dependence found for the elemental abundance during the CME and during the filament eruption could equally well be interpreted as a mass per charge dependence, inferring the charge from the type of solar wind. The ^{3}He-rich flares, i.e., impulsive flares, usually show enhancements of heavy elements, with Fe/O abundance ratios up to one [*Meyer*, 1985; *Reames*, 1992]. The enhancement in impulsive flares is monotonic with mass, which is called mass bias, and results from the ion acceleration process that depends on the mass per charge of an ion as well as its velocity. However, whether the low energies of the observed particles (typically 1 keV/nucleon) are sufficient to achieve the observed change in composition due to fractionation in the acceleration process remains to be demonstrated. Another concept that could explain the observed mass fractionation is diffusion across magnetic field lines. This is our favored concept to explain the observations, as discussed in detail below.

2. Disintegration of a Loop

The January 6, 1997, CME is associated with a large filament structure on the solar surface (S24° W10° [*Webb et al.*, 1998]), since this filament is located where the projection of the CME trajectory maps back on to the solar surface. There is no other feature visible on the solar disk that could possibly be responsible for the CME release. After all, this CME event occurred around solar minimum. Neither flare activity [*Hudson et al.*, 1998] nor energetic particles [*Cane et al.*, 1998; *Torsti et al.*, 1998] have been observed in connection with this CME, making the CME an even more unusual event. A filament on the solar surface with a length of $\sim 1.5 \times 10^5$ km went through considerable change during the days before the assumed release of the CME [*Webb et al.*, 1998]. The filament existed several days after the CME left the solar surface and was even the presumed starting location for a later CME on February 7, 1997 [*Webb et al.*, 1998]. Thus we cannot directly link the disintegration of this filament with the observed CME but possibly with the disintegration of parts of this filament structure. Careful inspection of the Yohkoh images of the zoo of loops of the filament structure revealed that a subset of these loops at the northwest end of the filament, a loop structure of about a quarter of the size of the filament, was missing after the release of the CME. There was no other feature in that area on the solar surface identified so far, which can be considered a candidate for a precursor to the CME. Thus, in the following we will base the interpretation of our observations on the disintegration of loops. It is well established that CMEs arise preferentially from closed magnetic field regions in the solar atmosphere where the field normally is sufficiently strong to constrain the coronal plasma from expanding outward into the heliosphere [*Gosling*, 1997]. Moreover, many of the ejections have the appearance of closed magnetic loops attached to the Sun at both ends [*Gosling*, 1997]. So far, the fundamental question of what causes the eruption of a CME is unanswered. Extensive computer modeling efforts [e.g., *Mikic and Linker*, 1997] as well as theoretical investigations [e.g., *Chen*, 1997] currently under way are aimed at understanding how a CME is actually released. Computer modeling shows that increased magnetic shear in the coronal loop will lead to instability, if a critical shear is exceeded, and eventually will launch a CME into interplanetary space [*Mikic and Linker*, 1997]. In addition to this slow increase of magnetic energy in a loop due to the energy deposited by shearing, there also exists an alternative concept of injecting magnetic energy into an existing loop structure, driving the structure out of equilibrium and leading to disintegration [*Chen*, 1997].

Our model of the CME event is as follows. A loop emerges from the solar surface and takes with it photospheric material. Owing to the expansion of the cross section of a part of the loop with height [*Chen*, 1997], a magnetic bottle is established between the two footpoints, which traps electrons and ions inside this structure. The confinement of plasma in a magnetic bottle is imperfect, because there is always a loss cone in velocity space from which ions can escape. Note that the particle losses through the loss cone are independent of the mass or charge of the particle [*Chen*, 1984] and therefore cannot cause fractionation. The loop heats up, and the hot electrons subsequently bring the trapped ions into higher ionization states corresponding to the temperature of the electrons in the loop. Most likely, the electron distribution in the loop will be non-Maxwellian, that is, will contain high-energy tails due to heating by plasma waves, since this is generally observed in space plasmas [see *Ma and Summers*, 1999, and references

therein]. Non-Maxwellian electron distributions are one of the ingredients of our model. Many loops along the filament were observed with the Yohkoh SXT instrument, which mainly observes radiation resulting from an electron plasma of 3–5 MK temperature. Thus one can safely assume the validity of the hot loop model [*Bray et al.*, 1991]. The foot points of the loop move, and if this movement winds up the magnetic field lines of a loop enough, the loop will disintegrate and set free the trapped plasma material into an expansion into space. Let us assume that the disintegrated loop evolves to be the CME. This CME will be observed first by SOHO/UVCS as a halo CME propagating toward the Earth and will later be detected in situ in the particle data with the SOHO/CELIAS instrument. Of course, a single loop will not release sufficient material to account for the mass of the CME as it was observed. It will take many loops disintegrating at the same time to come up with the mass. From the sequence of images of the filament one can deduce substantial activity on this part of the solar surface. Since the filament could be observed on the solar surface for more than 10 days before the release of the CME (the filament became visible on the east limb of the Sun on the morning of December 28, 1996), the loops will also have existed for a comparable time. The plasma inside is trapped by the magnetic bottle structure of the loop.

3. The Model

Diffusion across magnetic field lines due to isotropic scattering is described with the corresponding diffusion coefficient [*Chen*, 1984]

$$D_T = \frac{D_0}{1+\omega_c^2/\nu^2} \tag{1}$$

with

$$\omega_c = \frac{Ze}{m}B$$

the cyclotron frequency of an ion with a mass m and charge Ze in a magnetic field B; ν is the collision frequency, which is the inverse of the time between two collisions. D_0 is the diffusion coefficient parallel to the magnetic field, and e is the elementary charge. Assuming Coulomb collisions, the collision frequency for ion-ion collisions is [*Burgers*, 1969; *Peter*, 1996]

$$\nu_{jk} = \frac{16}{3}\frac{\sqrt{\pi\mu_{jk}}}{m_j}\left(\frac{Z_jZ_ke^2}{4\pi\varepsilon_0}\right)^2 (2k_BT_{jk})^{-\frac{3}{2}} \ln\Lambda\, n_k \tag{2}$$

with Z_j and Z_k the charges of the ions j and k with the respective masses m_j and m_k, ε_0 the vacuum dielectric constant, k_B the Boltzmann constant, and $\ln\Lambda$ the Coulomb logarithm. The main collision partners are assumed to be protons; thus $Z_k = 1$, $m_k = m_p$, and $n_k = n_p$, the proton density. Collisions between heavy ions are not considered here because of their low density and hence low collision frequency. Furthermore,

$$\mu_{jk} = \frac{m_jm_k}{m_j+m_k}$$

is the reduced mass of the collision partners, and

$$T_{jk} = \mu_{jk}\left(\frac{T_j}{m_j}+\frac{T_k}{m_k}\right)$$

is the reduced temperature. The diffusion coefficient for species i is [*Chen*, 1984]

$$D_{0,i} = \frac{k_BT_{ik}}{m_i\nu_{ik}}. \tag{3}$$

Now we have all the ingredients to evaluate diffusion across magnetic field lines (e.g., (1)). In Figure 1, diffusion coefficients for diffusion across magnetic field lines are shown for the hot loop model, using parameters that have been reported to be typical for this scenario [*Bray et al.*, 1991]. For the data presented in Figure 1 the assumed ion and proton temperatures are $T_i = T_p = 10^4$ K, the magnetic field strength is $B = 10^{-3}$ T, and the proton density is $n_p = 4\times10^{16}$ m^{-3}. We find a considerable mass dependence in the diffusion coefficients, such that the lighter ions diffuse out of the loop more easily than the heavier ions. Thus the plasma inside the loop becomes more and more depleted of lighter ions with time.

The ion temperature for both collision partners of 10^4 K assumed in this example is of rather low value. The ions will get heated later in the corona, starting at an altitude of around one solar radius above the solar surface [*Kohl et al.*, 1998], presumably by ion-cyclotron resonant Alfvén waves (see recent review on this topic [*Wurz and Gabriel*, 1999, and references therein]). The dependence on the temperature of the heavy ions is small because the reduced temperature, which is the quantity entering the equations (see (2) and (3)), is dominated by the proton temperature.

The mass dependence of the diffusion coefficients is not limited to the chosen set of parameters, which we shall discuss in some detail in the following. The mass dependence can be expressed as the ratio of the diffusion coefficients. In the case of $\omega_{c,i}^2 \gg \nu_{ip}^2$ we find that

$$\frac{D_T(i)}{D_T(j)} = \sqrt{\frac{m_i}{m_j}\frac{m_j+m_p}{m_i+m_p}}. \tag{4}$$

For oxygen and iron this evaluates to $D_T(\mathrm{O})/D_T(\mathrm{Fe}) = 0.979$ and corresponds to a condition of a strong magnetic field with no resulting fractionation. In the case of $\omega_{c,i}^2 \ll \nu_{ip}^2$ we find that

$$\frac{D_T(i)}{D_T(j)} = \sqrt{\frac{m_j}{m_i}\frac{m_i+m_p}{m_j+m_p}}\left(\frac{Z_j}{Z_i}\right)^2. \tag{5}$$

For oxygen and iron (O^{6+} and Fe^{10+} in our example)

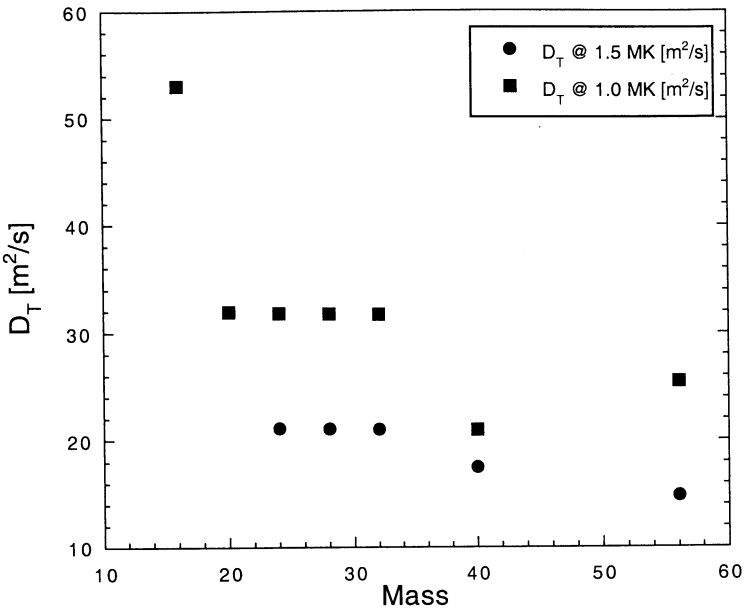

Figure 1. Diffusion coefficients for diffusion across magnetic field lines using the parameters (hot loop model): $T_i = T_p = 10^4$ K, $B = 10^{-3}$ T, $n_p = 4 \times 10^{16}$ m^{-3}, $T_e = 10^6$ K (circles) and $T_e = 1.5 \times 10^6$ K (squares). Only the most important charge state has been considered for each element. For oxygen and neon the diffusion coefficients are the same for the two electron temperatures.

this evaluates to $D_T(\mathrm{O})/D_T(\mathrm{Fe}) = 2.84$. This corresponds to the limit of strong mass fractionation for a given ionization state of the ions. Note the simplicity of (4) and (5) for the two extreme cases where only the masses and charges enter. The condition $\omega_{c,i}^2 \ll \nu_{ip}^2$ is fulfilled if the proton density n_p exceeds a critical density which is related to the proton temperature by

$$n_p > \frac{3B(2\pi k_B)^{3/2}\varepsilon_0^2}{\sqrt{\mu_i} Z_i Z_p^2 \Lambda e^3} T_p^{3/2}. \quad (6)$$

For our example we find that if $n_p \approx 3 \times 10^{10}\, T_p^{3/2}$ or exceeds this value for oxygen (with the density n_p in m^{-3} and the proton temperature T_p in K), we obtain strong mass fractionation. For heavier elements the critical density is lower due to the factor $\sqrt{\mu_i}$ in the denominator of (6). This critical density does not represent a sharp cutoff but the end of a rather smooth transition from a nonfractionating plasma loop to strong mass fractionation. For thermal equilibrium between the ions ($T_{ip} = T_{jp} = T$) the exact formula is

$$\frac{D_T(i)}{D_T(j)} = \sqrt{\frac{m_j}{m_i}\frac{m_i + m_p}{m_j + m_p}} \cdot \frac{N_p^2 Z_j^2 Z_p^4 \Lambda^2 e^6 + 9B^2(2\pi k_B T)^3 \varepsilon_0^4/\mu_{jp}}{N_p^2 Z_i^2 Z_p^4 \Lambda^2 e^6 + 9B^2(2\pi k_B T)^3 \varepsilon_0^4/\mu_{ip}}, \quad (7)$$

which simplifies to (4) and (5) for the two extreme cases. A numerical evaluation of (7) is shown in Figure 2 where the ratio $D_T(i)/D_T(j)$ is plotted for oxygen and iron ions as a function of the proton density. In the extreme case of temperature equilibrium between coronal electrons and protons, i.e., $T_p = T_e \approx 10^6$ K, a strong mass dependence in the diffusion coefficients is obtained for $n_p \approx 3 \times 10^{19}$ m^{-3}.

The dependence of the fractionation on the magnetic field strength can be seen in (6) and (7). As long as the magnetic field is weak enough such that $\omega_{c,i}^2 \ll \nu_{ip}^2$ is fulfilled, there is no dependence of the ratio of the diffusion coefficients on the magnetic field, and the fractionation is given by (5). For higher magnetic fields the difference in the diffusion coefficient between the light and heavy ions becomes smaller until it vanishes around $B = 0.01$ T in our example, a field strength which is a factor of ten higher than is considered a typical field strength in a hot loop [*Bray et al.*, 1991].

For the electron temperature, which governs the ionization state of the ions ($Z_k = Z_k(T_e)$), two cases are presented in Figure 1: $T_e = 1.0 \times 10^6$ K and $T_e = 1.5 \times 10^6$ K. The electron temperature is not a very critical parameter, although it has to be sufficiently high to have the elements ionized up to high charge states. High ion charge states are obtained either if the bulk electron plasma is at temperatures $T_e > 1$ MK or if at least a fraction of the electron plasma is at such temperatures (e.g., non-Maxwellian electron distributions). We will discuss the electron temperature, and in particular the effect of non-Maxwellian electron distributions, in more detail later in this paper. Note that in any case we need hot loops to explain the measured data. For an

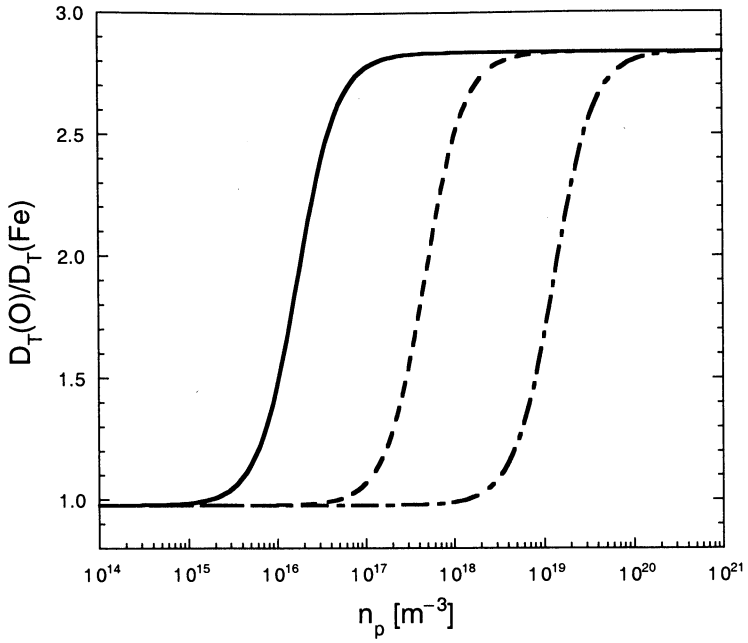

Figure 2. Ratios $D_T(\mathrm{O})/D_T(\mathrm{Fe})$ as a function of the proton density n_p for three values of the proton temperature (solid line $T_p = 10^4$ K, dashed line $T_p = 10^5$ K, and dashed-dotted line $T_p = 10^6$ K). The other parameters are the same as in Figure 1. The plateaus at low and high proton densities are given by (4) and (5) as 0.979 and 2.84, respectively.

electron temperature of 10^4 K, as would be the case in the cold loop model, the diffusion coefficients for each element are all the same since $Z_i \approx Z_j \approx 1$, and (7) (and (5) as well) simplifies to

$$\frac{D_T(i)}{D_T(j)} = \sqrt{\frac{m_j}{m_i}\frac{m_i + m_p}{m_j + m_p}}$$

despite that one requirement for strong fractionation is fulfilled ($\omega_{c,i}^2 \ll \nu_{ip}^2$). Thus we have about the same diffusion coefficients for all elements, and we cannot explain the mass-dependent fractionation we observe with the cold loop model.

If the material contained in the loop eventually becomes the observed CME, the observed mass fractionation can be explained, at this point only qualitatively, by the different losses of the various heavy ions contained in the loop. Even the mass dependence of the diffusion coefficient we find, with an increasing reduction of the lighter ions and an almost constant diffusion coefficient for silicon and heavier ions, appears to be just the inverse of the observed fractionation. Assuming that diffusion across magnetic field lines is the relevant physical process to explain our observational data results in the fractionation being according to mass per charge rather than being a plain mass fractionation.

An additional effect altering the composition of a flux tube may arise from the curvature and the gradient of the magnetic field of a flux tube [*Jackson*, 1983], which causes an average ion drift in the direction of the gradient and curvature of the magnetic field. This drift velocity is proportional to q^{-1} of the ion and thus favors the loss of lighter ions since their charge is smaller at the considered temperatures. For the geometry and the magnetic fields of typical flux tubes the associated drift velocities are very small ($\sim 10^{-3}$ m/s) and the resulting fractionation is small as well.

Having derived the diffusion coefficients we can pursue the model one step further by trying to derive a quantitative fractionation of the elements. We assume a loop of cylindrical cross section and calculate the loss of a specific element with time due to the diffusion across magnetic field lines. The loop geometry is defined as a tube of diameter $2a$ with a density of n_0 of a specific element inside the tube

$$n(r,0) = \begin{cases} n_0 & : \quad 0 \le |r| < a \\ 0 & : \quad a \le |r| \le \infty. \end{cases} \tag{8}$$

Outside the tube is vacuum

$$n(a,t) = 0. \tag{9}$$

For this problem we have to solve the diffusion equation, which is performed in cylindrical coordinates

$$\frac{\partial n}{\partial t} = D_T \frac{1}{r}\frac{\partial}{\partial r}\left(r\frac{\partial n}{\partial r}\right) = D_T\left(\frac{\partial^2 n}{\partial r^2} + \frac{1}{r}\frac{\partial n}{\partial r}\right), \tag{10}$$

and we assume only a radial dependence. No dependence along the loop or as a function of azimuth angle

is considered. Using Skylab data, *Foukal* [1976] found that for coronal loops "the emission in loops often was reasonably unchanged along their length", which gives some justification to our simple one-dimensional model. Moreover, coronal loops typically show only one temperature along their full length [*Kjeldseth-Moe and Brekke*, 1998; *Lenz et al.*, 1999].

We solve (10) by using the Laplace transformation (see Appendix A) and obtain

$$n(r,t) = n_0 \sum_{j=1}^{\infty} \frac{2}{\alpha_j} e^{-(\alpha_j/a)^2 D_T t} \frac{J_0\left(\alpha_j \frac{r}{a}\right)}{J_1(\alpha_j)} \tag{11}$$

with J_0 and J_1 the Bessel functions of zeroth and first order, and α_j the jth zero of J_0 (i.e., $J_0(\alpha_j) = 0$). Equation (11) is an exact solution of our problem and a convergent sum. Typically, we are interested in long time periods, so we only need to consider a few terms of the sum in (11), because of the exponential term. To compare the calculations with the reported measurements [*Wurz et al.*, 1998] we need to integrate (11) over the entire flux tube

$$\begin{aligned} N(t) &= 2\pi \int_0^a n(r,t) r dr \\ &= \sum_{j=1}^{\infty} \frac{4\pi n_0}{\alpha_j J_1(\alpha_j)} e^{-(\alpha_j/a)^2 D_T t} \int_0^a J_0\left(\alpha_j \frac{r}{a}\right) r dr, \end{aligned} \tag{12}$$

which resolves to

$$N(t) = n_0 \sum_{j=1}^{\infty} \frac{4\pi a^2}{\alpha_j^2} e^{-(\alpha_j/a)^2 D_T t}. \tag{13}$$

Using the initial number of ions $N_0 = \pi a^2 n_0$, we can write (13) as

$$N(t) = N_0 \sum_{j=1}^{\infty} \frac{4}{\alpha_j^2} e^{-(\alpha_j/a)^2 D_T t}. \tag{14}$$

The test of (14) for $t \to 0$ gives

$$\lim_{t \to 0} N(t) = N_0 \sum_{j=1}^{\infty} \frac{4}{\alpha_j^2} = N_0$$

since $\sum_{j=1}^{\infty} \alpha_j^{-2} = 1/4$ [*Prudnikov et al.*, 1986].

Having found an analytic expression for the fractionation (equation (14)) we can investigate what is the crucial parameter of a particle governing the fractionation. For that purpose we consider only the first summand in (14) for the fractionation

$$f_i(t) = \frac{N_i(t)}{N_{0,i}} \approx \frac{4\pi a^2}{\alpha_0^2} e^{-(\alpha_0/a)^2 D_{T,i} t}$$

and build the ratio of fractionations for two different elements

$$\begin{aligned} \frac{f_i(t)}{f_j(t)} &\approx \frac{e^{-(\alpha_0/a)^2 D_{T,i} t}}{e^{-(\alpha_0/a)^2 D_{T,j} t}} \\ &= e^{-(\alpha_0/a)^2 (D_{T,i} - D_{T,j}) t} \end{aligned}$$

to assess the fragmentation changing with the element. The difference in fragmentation is given by the difference in diffusion coefficients. In the case that $\omega_{c,i}^2 \ll \nu_{ip}^2$ we get

$$\begin{aligned} &D_{T,i} - D_{T,j} \\ &= \frac{3(2\pi)^{3/2} (k_B T)^{5/2} \varepsilon_0^2}{n_p Z_p^2 \Lambda e^4} \left(\frac{1}{\sqrt{\mu_{ip}} Z_i^2} - \frac{1}{\sqrt{\mu_{jp}} Z_j^2} \right) \end{aligned} \tag{15}$$

From (15) it is clear that the fractionation of species is mainly governed by the different ionization state the species are in. The mass of the particle has a minor effect on the fractionation. This can already be inferred from (5).

Now we can evaluate (14) for the different elements. We simply investigate the depletion each ion species suffers in the proton plasma, i.e., the fractionation $N(t)/N_0$, due to diffusion perpendicular to the magnetic field lines as a function of time. This makes the analysis independent of any assumptions on the initial abundance of the elements (for example, the photospheric abundance). By multiplying with an initial density for an element we will get the final abundances of elements at the time of the release of the CME. However, coming up with an initial abundance is an involved endeavor and is not required here to explain the observed mass fractionation. Also, we can assume that these initial elemental abundances are modified by the FIP effect, given the closeness of this region to the solar equator.

From (2) it is clear that the diffusion coefficient strongly depends on the ionization state of a particular ion. Therefore a good knowledge of the charge state distribution of an ion is important. Thus, for each element we first calculate its charge state distribution for a given electron temperature T_e by solving

$$\begin{aligned} \tfrac{d}{dt} n_0 &= n_e \left(-n_0 C_0 + n_1 R_1\right) \\ &\vdots \\ \tfrac{d}{dt} n_i &= n_e \left(n_{i-1} C_{i-1} - n_i C_i - n_i R_i + n_{i+1} R_{i+1}\right) \\ &\vdots \\ \tfrac{d}{dt} n_k &= n_e \left(n_{k-1} C_{k-1} - n_k R_k\right). \end{aligned} \tag{16}$$

We solved this set of $k+1$ ordinary differential equations by numerical integration using a fifth-order Cash-Karp Runge-Kutta method until ionization equilibrium is reached. The n_i values are the densities for an element for all of its possible charge states (from 0 to k), and n_e is the electron density (with $n_e = n_p$). $C_i = C_i(T_e)$ and $R_i = R_i(T_e)$ are the total ionization

rate and the recombination rate, respectively, for an ion in charge state i for which we use the rates given by *Arnaud and Rothenflug* [1985] and *Arnaud and Raymond* [1992]. Typically, a stable solution, that is ionization equilibrium, is reached after less than 10-s integration time.

Since it is unreasonable to think that the proton temperature and the electron temperature are not in thermal equilibrium (that is, we have $T_e = T_p = T_i$) for the time scales which are of interest for us, we have to assume that non-Maxwellian tails in the electron distribution (e.g., Kappa distributions instead of Maxwellian distributions) will be responsible for the formation of the highly charged ions that are observed. As a good approximation, these non-Maxwellian electron distributions can be described by the sum of two Maxwellian distributions: a core distribution with the proton temperature $T_{e,core} = T_p$, and a halo distribution of much higher temperature $T_{e,halo}$ and with a density of a few percent of the core distribution. Actually, measurements of the electron distributions in the CME plasma at 1 AU show a two-component plasma that can be described well by the sum of two Maxwellian distributions of a cold and dense core plasma and a hot halo plasma of much lower density [*Larson et al.*, 2000]. The idea of double-Maxwellian electron distributions was employed before for the calculation of the ionization balance of coronal plasma and compared with a calculation using Kappa distributions, which showed that these two approaches give very similar results [*Aellig et al.*, 1999]. The advantage of using double-Maxwellian distributions is that we can still use the ionization rates and the recombination rates given in *Arnaud and Rothenflug* [1985] and *Arnaud and Raymond* [1992], which were derived for Maxwellian electron distributions. Of course, we have to modify (16) to the double-Maxwellian electron distribution, which is straightforward. The result of such a calculation is shown in Figure 3 for oxygen using $T_{e,core} = 10^5$ K and $T_{e,halo} = 2 \times 10^6$ K for various densities of the halo population with respect to the total electron density. Also, the result for a single Maxwellian distribution for a temperature of 2 MK is given for comparison. The effect of the double-Maxwellian distribution is of course that the final charge state distribution is centered at lower charge states than for the single hot Maxwellian because of recombination of ions with the colder electrons.

Once we have the charge state distributions we can proceed to derive a set of diffusion coefficients (equation (1)) and then a set of fractionations (equation (14)) for the individual charge states of each element. The weighted sum of the latter then gives the fractionation for an element. Remember that for each element, ions of lower ionization state are preferentially lost compared to the higher charged ions. The model parameters have been varied within some limits to reproduce the measured fractionation data as well as possible. A good agreement was found for a proton density of $n_p = 4.6 \times 10^{17}$ m^{-3}, an electron temperature of the halo distribution $T_{e,halo} = 2.1 \times 10^6$ K and an integra-

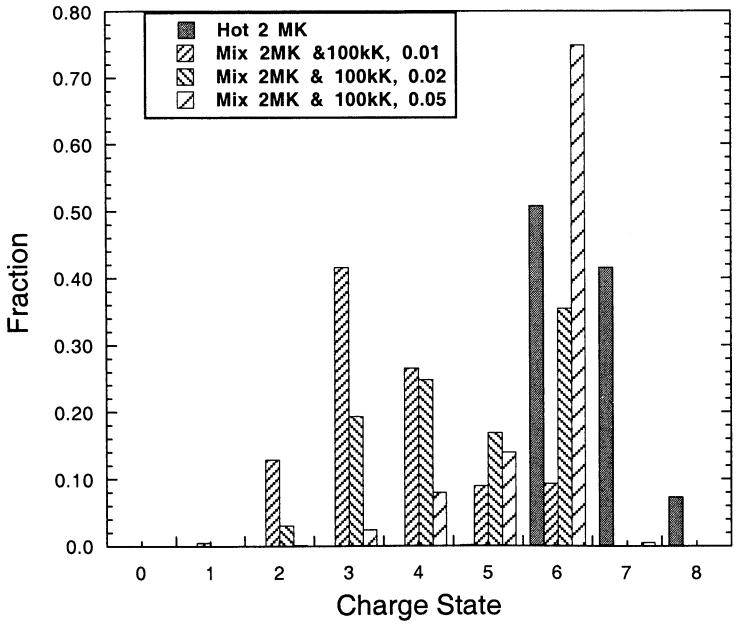

Figure 3. Charge state distributions for oxygen obtained by integrating (16) until a steady state solution is reached. The distribution labeled "Hot 2 MK" is for a single electron plasma at 2 MK; the other three distributions labeled "Mix 2 MK & 100 kK" are calculated for double-Maxwellian distributions with $T_{e,core} = 10^5$ K and $T_{e,halo} = 2 \times 10^6$ K for densities with respect to the total electron density of 1, 2, and 5%, respectively.

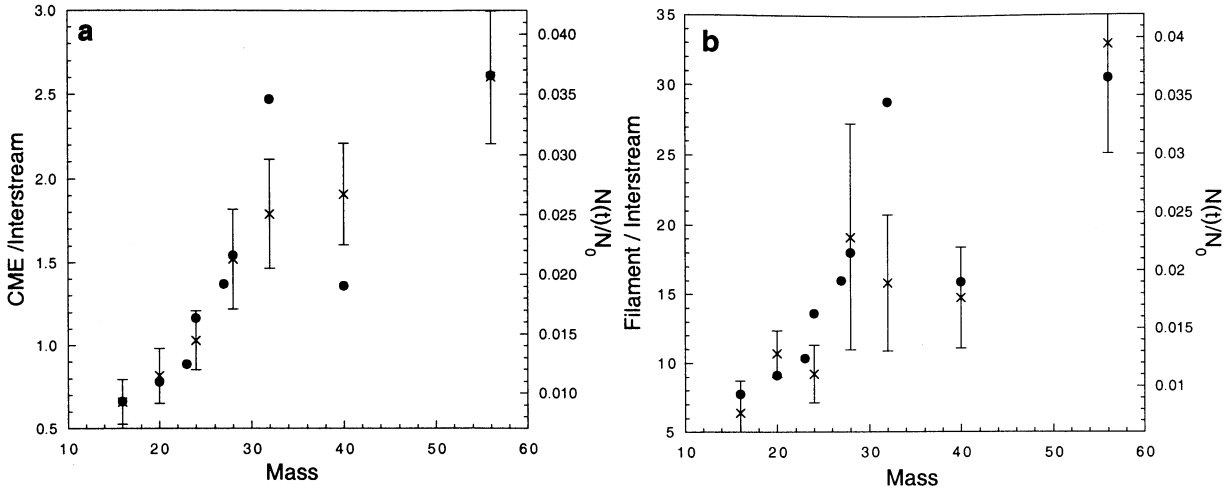

Figure 4. Comparison of the observed elemental fractionation (a) in the CME and (b) the filament with respect to the interstream elemental abundances before the event [*Wurz et al.*, 1998], with the result from the calculation of the depletion of elements due to diffusion across magnetic field lines. For the model calculation a time of 27.5 hours has been used. For the measured data the y axis is always on the left (crosses with error bars) and for the calculated data the y axis is on the right (circles). The range of the left and right y axes for each plot is set such that they span the same factor between minimum and maximum.

tion time in (14) of $t = 27.5$ hours. The proton, ion, and electron temperatures, the magnetic field strength, and the flux tube radius have been fixed beforehand to $T_i = T_p = T_{e,core} = 10^5$ K, $B = 10^{-3}$ T, and $a = 10^4$ m. The comparison of the measured elemental fractionation in the CME and in the filament with the fractionation due to diffusion across magnetic field lines is shown in Figures 4a and 4b, respectively. The crosses with the error bars are the measured data from *Wurz et al.* [1998] (the pertaining y axis is on the left side of Figures 4a and 4b). The results from the model calculation are indicated by the circles (the pertaining y axis is on the right side of Figures 4a and 4b). The left and right y axes are chosen such that they span the same relative range between minimum and maximum value, a factor of 6 for the CME (Figure 4a), and a factor of 7 for the filament (Figure 4b).

4. Discussion

The fractionation data shown in Figure 4 are obtained after a time of 27.5 hours for which the loop system must have existed in a stable fashion during which the diffusion changed the elemental abundances. Note that this time scales with the strength of the magnetic field and the diameter of the tube. For lower fields or for thinner tubes we need shorter times to obtain the fractionation. Moreover, recall that the loop system (the active region) was observed on the solar disk for at least two solar rotations. Hot coronal loops (hot loops) are stable for typically 4–5 hours [*Kjeldseth-Moe and Brekke*, 1998], which agrees with earlier observations of hot loops associated with Sun spots [*Foukal*, 1976]. However, hot coronal loops with lifetimes of days have also been observed at visible and X-ray wavelengths [*Bray et al.*, 1991]. Thus the 27.5 hours needed in our case to come up with the elemental fractionation appear to be not so unusual, but this time is longer than the typical lifetime of a hot loop. This could be the reason why for most of the observed CMEs such a strong elemental fractionation has not been observed. However, for the November 1997 CME, strong enrichments for iron have also been observed [*Wimmer-Schweingruber et al.*, 1999]. Transition zone loops show much higher variability on timescales down to minutes [*Kjeldseth-Moe and Brekke*, 1998] and have therefore been excluded from our considerations. Their temperatures would also be too low.

One additional result of this study is that one has to be very careful when deriving electron temperatures from the population of various charge states of an element (e.g., using O^{5+} and O^{6+}). Compared to the case of a Maxwellian electron plasma, the charge state distributions in loops are altered in two ways: first, by the non-Maxwellian electron distributions and second, by the different losses by diffusion perpendicular to the magnetic field lines. Together, these processes will result in a severe overestimation of the temperature of the electron plasma. Although the main electron plasma is only at 10^5 K, O^{5+} and O^{6+} ions can be observed indicating a million-degree plasma (see Figure 3) using the conventional interpretation. Diffusion perpendicular to the magnetic field lines will even enhance this effect because ions in lower ionization states are preferentially lost from the loop. The latter process will gain importance the longer the plasma is confined in the loop.

These effects may also be the explanation why the very same coronal loop can be "seen in largely different temperatures," that is, in optical emission lines from ions excited at different electron temperatures [*Kjeldseth-Moe and Brekke*, 1998].

If one wants to push the idea of disintegrating loops as the initial step of a CME release further, one could possibly explain the variety in the composition observed in CMEs. Given the variety of loops, in terms of temperature, size, and many other parameters [*Bray et al.*, 1991], and the temporal development of the elemental abundance, or the development of the charge distribution, one can easily explain many observations of CMEs by finding the proper initial conditions in a loop system on the solar surface, which will eventually evolve in the CME to the final observed plasma composition.

In the above calculation we used only an electron distribution described by two Maxwellian distributions, with $T_{e,core}$ and $T_{e,halo}$ being the same for all elements to derive the charge state distribution of an element. It is known that the charge state distribution for different elements is governed by different electron temperatures, or rather the balance between ionization and recombination for a particular charge state of an element is reached at different electron temperatures [see, e.g., *Geiss et al.*, 1995; *von Steiger*, 1995].

In conclusion, the model presented above could be improved by elaborating on some details, and possibly by treating this problem in two or three dimensions. It is anticipated that an improved model will reproduce the observed elemental fractionation even better. However, already at this stage the model can explain the observed mass-dependent fractionation, with a monotonic increase toward heavier elements. Furthermore, the model can also explain the magnitude of the fractionation, with the Si/O and Fe/O abundance ratios being about a factor of 4 higher than those observed in regular slow solar wind. The parameters for the model to reproduce the measured data can vary in a certain range, and we chose values located in the middle of the possible parameter space. For example, with the set of parameters used for Figure 2 a comparable agreement with the measured data is found; however, the integration time has to be increased to 7 days in this case.

Appendix A

Before we begin with the calculation, we introduce the variable transformation $n_s(r,t) = n_0 - n(r,t)$, which makes the calculations easier, and changes the boundary conditions (equations (8) and (9)) such that

$$n_s(r,0) = \begin{cases} 0 & : \quad 0 \le |r| < a \\ n_0 & : \quad a \le |r| \le \infty \end{cases} \qquad (A1)$$
$$n_s(a,t) = n_0.$$

To solve the diffusion equation (equation (10)), we apply the Laplace transform

$$\mathcal{L}\{f(t)\} = \int_0^\infty f(t)e^{-st}dt = \tilde{f}(s),$$

and we get

$$\frac{\partial^2 \tilde{n}_s}{\partial x^2} + \frac{1}{x}\frac{\partial \tilde{n}_s}{\partial x} - \tilde{n}_s = 0 \qquad (A2)$$

by using the substitution $x = r\sqrt{s/D_T}$. Note that in (A2) the elemental dependence is now contained in the variable x via the diffusion coefficient D_T. Equation (A2) is known as the modified Bessel differential equation and has the solution

$$\tilde{n}_s(\xi, s) = A(s)I_0(x) + B(s)K_0(x) \qquad (A3)$$

with $\xi = r/\sqrt{D_T}$, I_0 being the modified Bessel function, and K_0 being the modified Hankel function. The prefactor $B(s)$ is set to zero, since K_0 is divergent for $x \to 0$ (since $\lim_{x\to\infty} K_0(x) \approx \ln x$). The prefactor $A(s)$ is derived from the boundary condition specified by (A1)

$$\tilde{n}_s(\xi_0, s) = \int_0^\infty n_s(a,t)e^{-st}dt = \int_0^\infty n_0 e^{-st}dt = \frac{n_0}{s} \qquad (A4)$$

using $\xi_0 = a/\sqrt{D_T}$. Thus we obtain for the coefficient $A(s)$ in (A3)

$$A(s) = \frac{n_0}{s}\frac{1}{I_0(\xi_0\sqrt{s})} \qquad (A5)$$

and the solution of (A3) becomes

$$\tilde{n}_s(\xi, s) = \frac{n_0}{s}\frac{I_0(\xi\sqrt{s})}{I_0(\xi_0\sqrt{s})} = \frac{n_0}{s}\frac{J_0(i\xi\sqrt{s})}{J_0(i\xi_0\sqrt{s})}, \qquad (A6)$$

where J_0 is the Bessel function of the first kind. The solution in the time domain is obtained by inverse Laplace transformation of (A6)

$$n_s(r,t) = \frac{n_0}{2\pi i}\oint_C \frac{1}{s}\frac{J_0(i\xi\sqrt{s})}{J_0(i\xi_0\sqrt{s})}e^{st}ds \qquad (A7)$$

with the closed contour C of the contour integral given in Figure 5. The value of the contour integral in (A7) is obtained by the residue theorem

$$\frac{n_0}{2\pi i}\oint_C f(s)ds = n_0\sum_{k=1}^{n}\mathrm{Res}_f(s_k)$$

with the s_k values the points for which the function $f(s)$ is singular. The power series representation of $J_0(z)$ has only even powers of z, so we do not need to worry about branch cuts. There is a singularity at $s = 0$ in the argument of the integral of (A7), which evaluates to $\mathrm{Res}_f(s = 0) = 1$. The other singularities occur at the points s_j where $J_0(i\xi_0\sqrt{s_j}) = 0$. Since J_0 is analytic

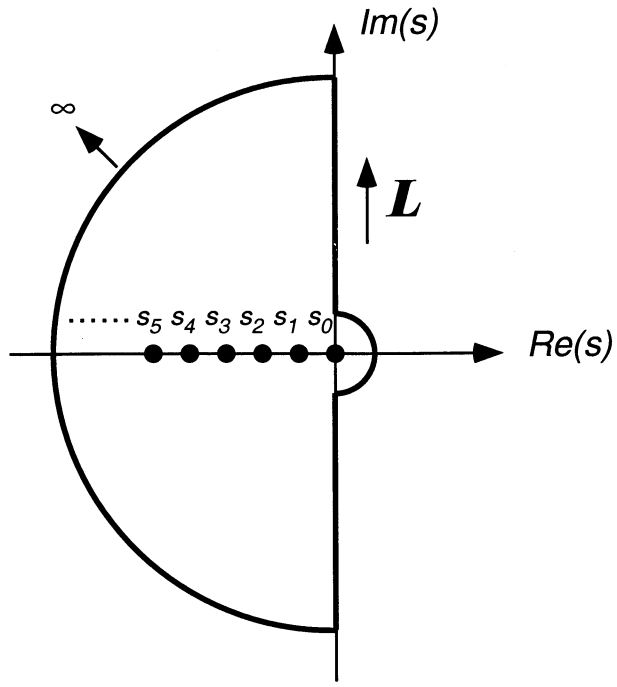

Figure 5. Contour path used for the integration in (A7), with the s_k values being the points for which the argument of the integral in (A7) is singular.

and the singularities are not at infinity, we can write

$$\begin{aligned} \mathrm{Res}_f(\alpha_j) &= \frac{\frac{1}{s_j} J_0\left(i\xi\sqrt{s_j}\right) e^{s_j t}}{\frac{d}{ds} J_0\left(i\xi_0\sqrt{s_j}\right)} \\ &= \frac{-\frac{\alpha_j^2}{\xi_0^2} J_0(\alpha_j \xi/\xi_0) e^{-(\alpha_j/\xi_0)^2 t}}{\frac{\xi_0^2}{2\alpha_j} J_1(\alpha_j)} \end{aligned} \tag{A8}$$

with α_j being the arguments for which the Bessel function is zero ($J_0(\alpha_j) = 0$) and therefore $s_j = -\alpha_j^2/\xi_0^2$. Using (A8) and undoing the substitution $n(r,t) = n_0 - n_s(r,t)$, we obtain as the solution of (10)

$$n(r,t) = n_0 \sum_{j=1}^{\infty} \frac{2}{\alpha_j} e^{-(\alpha_j/a)^2 D_T t} \frac{J_0\left(\alpha_j \frac{r}{a}\right)}{J_1(\alpha_j)}. \tag{A9}$$

Acknowledgments. The authors wish to acknowledge stimulating discussions with R. F. Wimmer-Schweingruber of the University of Bern, Bernhard Fleck of ESA/ESTEC, and Andreas Unterreiter of the University of Kaiserslautern. This work is supported by the Swiss National Science Foundation.

Michel Blanc thanks Leonard Burlaga and Rainer Schwenn for their assistance in evaluating this paper.

References

Aellig, M.R., P. Bochsler, H. Grünwaldt, S. Hefti, P. Wurz, M. Hilchenbach, D. Hovestadt, F.M. Ipavich, and F. Gliem, The influence of surprathermal electrons on the derivation of coronal electron temperatures from solar wind minor ion charge states, *Phys. Chem. Earth C*, *24*(4), 407–414, 1999.

Arnaud, M., and J. Raymond, Iron ionization and recombination rates and ionization equilibrium, *Astrophys. J.*, *398*, 394–406, 1992.

Arnaud, M., and R. Rothenflug, An updated evaluation of recombination and ionization rates, *Astron. Astrophys. Suppl. Ser.*, *60*, 425–457, 1985.

Bray, R.J., L.E. Cram, C.J. Durrant, and C.J. Loughhead, *Plasma Loops in the Solar Corona*, Cambridge Univ. Press, New York, 1991.

Burgers, J.M., *Flow Equations for Composite Gases*, Academic Press, San Diego, Calif., 1969.

Burlaga, L., R. Fritzenreiter, R. Lepping, K. Ogilvie, A. Szabo, A. Lazarus, J. Steinberg, G. Gloeckler, R. Howard, D. Michels, C. Farrugia, R.P. Lin, and D.E. Larson, A magnetic cloud containing prominence material: January 1997, *J. Geophys. Res.*, *103*, 277–286, 1998.

Cane, H.V., I.G. Richardson, and O.C. St.Cyr, The interplanetary events of January–May, 1997 as inferred from energetic particle data, and their relationship with solar events, *Geophys. Res. Lett.*, *25*(14), 2517–2520, 1998.

Chen, F.F., *Introduction to Plasma Physics and Controlled Fusion*, New York, Plenum Press, 1984.

Chen, J., Coronal mass ejections: Causes and consequences a theoretical view, in *Coronal Mass Ejections*, *Geophys. Monogr. Ser.*, vol. 99, edited by N. Crooker, J.A. Joselyn and J. Feynman, pp. 65–81, AGU, Washington, D.C., 1997.

Foukal, P.V., The pressure and energy balance of the cool corona over sunspots, *Astrophys. J.*, *210*, 575–581, 1976.

Fox, N.J., M. Peredo, and B.J. Thompson, Cradle to grave tracking of the January 6–11, 1997, Sun-Earth connection event, *Geophys. Res. Lett.*, *25*(14), 2461–2464, 1998.

Geiss, J., et al., The southern high-speed stream: Results from the SWICS instrument on Ulysses, *Science*, *268*, 1033–1036, 1995.

Gosling, J.T., Coronal mass ejections and magnetic flux ropes in interplanetary space, in *Physics of Magnetic Flux Ropes*, *Geophys. Monogr. Ser.*, vol. 58, edited by C.T. Russell, E.R. Priest and L.C. Lee, pp. 343–364, AGU, Washington, D.C., 1990.

Gosling, J.T., Coronal mass ejections: An overview, in *Coronal Mass Ejections*, *Geophys. Monogr. Ser.*, vol. 99, edited by N. Crooker, J.A. Joselyn and J. Feynman, pp. 9–16, AGU, Washington, D.C., 1997.

Hudson, H.S., J.R. Lemen, O.C. St.Cyr, A.C. Sterling, and D.F. Webb, X-ray coronal changes during hale CMEs, *Geophys. Res. Lett.*, *25*(14), 2481–2484, 1998.

Hundhausen, A., Coronal mass ejections, in *The Many Faces of the Sun*, edited by K.T. Strong, J.L.R. Saba, B.M. Haisch, and J.T. Schmelz, pp. 143–200, New York, Springer-Verlag, 1999.

Jackson, J.D., *Klassische Elektrodynamik*, Walter de Gruyter, New York, 1983.

Kjeldseth-Moe, O., and P. Brekke, Time variability of active region loops observed with the Coronal Diagnostic Spectrometer (CDS) on SOHO, *Sol. Phys.*, *182*(1), 73–95, 1998.

Kohl, J.L., et al., UVCS/SOHO empirical determinations of anisotropic velocity distributions in the solar corona, *Astrophys. J.*, *501*, L127–L131, 1998.

Larson, D.E., R.P. Lin, and J. Steinberg, Extremely cold electrons in the January 1997 magnetic cloud, *Geophys. Res. Lett.*, *27*(2), 157–160, 2000.

Lenz, D.D., E.E. DeLuca, L. Golub, R. Rosner, and J.A. Bookbinder, Temperature and emission-measure profiles along long-lived solar coronal loops observed with the

Transition Region and Coronal Explorer, *Astrophys. J.*, *517*, L155–L158, 1999.

Ma, C.-Y., and D. Summers, Formation of power-law energy spectra in space plasmas by stochastic acceleration due to whistler-mode waves, *Geophys. Res. Lett.*, *26*(8), 1121–1124, 1999.

Meyer, J.-P., The baseline composition of solar energetic particles, *Astrophys. J. Suppl. Ser.*, *57*, 151–171, 1985.

Mikic, Z., and J.A. Linker, The initiation of coronal mass ejections by magnetic shear, in *Coronal Mass Ejections*, *Geophys. Monogr. Ser.*, vol. 99, edited by N. Crooker, J.A. Joselyn and J. Feynman, pp. 57–64, AGU, Washington, D.C., 1997.

Peter, H., Mehrflüssigkeitsmodelle der unteren Sonnenatmosphäre und Schlußfolgerungen für den Sonnenwind, Rep. MPAE-W-100-97-06, Max-Planck-Inst. für Aeron., 1996.

Prudnikov, A.P., Yu.A. Brychkov, and O.I. Marichev, *Integral and Series*, vol. 2, *Special Functions*, pp. 690–691, Gordon and Breach Sci., New York, 1986.

Reames, D.V., Energetic particle observations and the abundance of elements in the solar corona, *Eur. Space Agency Spec. Publ.*, *ESA SP-348*, 315–323, 1992.

Torsti, J., A. Anttila, L. Kocharov, P. Mäkelä, E. Riihonen, T. Sahla, M. Teittine, E. Valtonen, T. Laitinen, and R. Vainio, Energetic ($\approx$ 1 to 50 MeV) protons associated with Earth-directed coronal mass ejections, *Geophys. Res. Lett.*, *25*(14), 2525–2528, 1998.

von Steiger, R., Solar wind composition and charge states, *Solar Wind Eight*, edited by D. Winterhalter, et al., pp. 193–198, AIP Press, College Park, Md., 1995.

Webb, D.F., E.W. Cliver, N. Gopalswamy, H.S. Hudson, and O.C. St.Cyr, The solar origin of the January 1997 coronal mass ejection, magnetic cloud and geomagnetic storm, *Geophys. Res. Lett.*, *25*(14), 2469–2472, 1998.

Wimmer-Schweingruber, R.F., O. Kern, and D.C. Hamilton, On the solar wind composition during the November 1997 solar particle events: WIND/MASS observations, *Geophys. Res. Lett.*, *26*(23), 3541–3544, 1999.

Wurz, P., et al., Elemental composition before, during, and after the January 6, 1997, CME event measured by CELIAS/SOHO, *Eur. Space Agency Spec. Publ.*, *ESA SP-415*, 395–400, 1997.

Wurz, P., et al., Elemental composition of the January 6, 1997, CME, *Geophys. Res. Lett.*, *25*(14), 2557–2560, 1998.

Wurz, P., and A.H. Gabriel, Wind acceleration processes: Rapporteur paper IV, *Proceedings of the SOHO-8 Workshop*, *Eur. Space Agency Spec. Publ.*, *ESA SP-446*, 87–95, 1999.

P. Bochsler and P. Wurz, Physics Institute, University of Bern, Sidlerstrasse 5, 3012 Bern, Switzerland. (peter.wurz@soho.unibe.ch; peter.bochsler@soho.unibe.ch)

M. A. Lee, Institute for the Study of Earth, Oceans and Space and Department of Physics, University of New Hampshire, Durham, NH 03824, USA. (marty.lee@unh.edu)

(Received May 18, 2000; revised August 7, 2000; accepted August 8, 2000.)